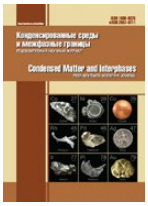

ISSN 1606-867X (Print)
ISSN 2687-0711 (Online)
Condensed Matter and Interphases
Kondensirovannye Sredy i Mezhfaznye Granitsy
https://journals.vsu.ru/kcmf/

Original articles

Research article
https://doi.org/10.17308/kcmf.2025.27/13014

Ternary molybdate $K_5Cu_{0.5}Hf_{1.5}(MoO_4)_6$: synthesis, structure, thermal expansion, and ionic conductivity

E. V. Kovtunets✉, T. S. Spiridonova, Yu. L. Tushinova, T. T. Bazarova, A. V. Logvinova, B. G. Bazarov

Baikal Institute of Nature Management, Siberian Branch of the Russian Academy of Sciences, 6, Sakhyanova st., 670047 Ulan-Ude, Republic of Buryatia, Russian Federation

Abstract

Objective: A novel ternary molybdate, $K_5Cu_{0.5}Hf_{1.5}(MoO_4)_6$, was synthesized using a solid-state ceramic method. The sequence of chemical transformations involved in its formation was determined, revealing that the compound undergoes incongruent melting at 634 °C.

Experimental: The crystal structure was refined using the Rietveld method, revealing a trigonal structure (space group $R\bar{3}c$) with unit cell parameters a = 10.5617(2) Å; c = 37.5017(7) Å; V= 3622.9(1) Å^3, R_{wp} = 3.78. Attenuated total reflection Fourier-transform infrared (ATR-FTIR) spectroscopy confirmed the presence of isolated MoO_4 tetrahedra. The electrical conductivity of the title compound reached $7.5 \cdot 10^{-4}$ S/cm at 550°C, with an activation energy of E_a = 0.9 eV. Thermal deformations were investigated by high temperature powder X-ray diffraction (HT-XRD) over the temperature range of 30–500 °C.

Results: $K_5Cu_{0.5}Hf_{1.5}(MoO_4)_6$ was classified as a high thermal expansion material ($\alpha_V = 45 \times 10^{-6}$ °C^{-1} at 500 °C), and exhibited low anisotropy. Combined results from electrochemical impedance spectroscopy (EIS) and HT-XRD indicated that the endothermic peak observed at 479 °C in the differential scanning calorimetry (DSC) curve corresponded to a first-order phase transition.

Keywords: Potassium; copper; Hafnium; Ternary molybdate; Synthesis; Crystal structure; Thermal expansion; Ionic conductivity

Funding: This research was conducted within the framework of the state assignment to Baikal Institute of Nature Management SB RAS (No. 0273-2021-0008) and was supported by the Russian Science Foundation (project No. 23-29-00327).

Acknowledgments: The studies involving XRD, thermal analysis, ATR-FTIR, HT-XRD, and conductivity measurements were performed using the resources of the Research Equipment Sharing Center of BINM SB RAS.

For citation: Kovtunets E. V., Spiridonova T. S., Tushinova Yu. L., Bazarova Ts. T., Logvinova A. V., Bazarov B. G. Ternary molybdate $K_5Cu_{0.5}Hf_{1.5}(MoO_4)_6$: synthesis, structure, thermal expansion and ionic conductivity. *Condensed Matter and Interphases*. 2025;27(3): 380–390. https://doi.org/10.17308/kcmf.2025.27/13014

Для цитирования: Ковтунец Е. В., Спиридонова Т. С., Тушинова Ю. Л., Базарова Ц. Т., Логвинова А. В., Базаров Б. Г. $K_5Cu_{0.5}Hf_{1.5}(MoO_4)_6$: синтез, структура, термические деформации и ионная проводимость. *Конденсированные среды и межфазные границы*. 2025;27(3): 380–390. https://doi.org/10.17308/kcmf.2025.27/13014

✉ Evgeniy V. Kovtunets, e-mail: kovtunets@binm.ru

1. Introduction

Progress in modern materials science is closely linked to advances in the synthesis and characterization of complex inorganic oxides. Ternary molybdates and tungstates are particularly promising due to their structural versatility, tunable cation compositions, and a wide range of functional properties, including ferroelectricity [1], piezoelectricity [2], luminescence [3, 4], laser activity [5,6], photocatalysis [7], magnetism [8], antiferromagnetism [9], and ionic conductivity [10–14]. The crystal structures of this class of compounds typically form three-dimensional frameworks containing numerous cavities and interconnected channels, constructed from metal polyhedra and EO_4 tetrahedra (E = Mo, W). Among them are representatives of well-known structural types such as NASICON [15], scheelite [16], alluaudite [17], glaserite [18], lyonsite [19], and others [20].

In the present study, the family of ternary molybdates with the general formula $M^{I}_5M^{II}_{0.5}M^{IV}_{1.5}(MoO_4)_6$ [21–29] is extended through the synthesis of $K_5Cu_{0.5}Hf_{1.5}(MoO_4)_6$. A preliminary characterization of this compound was performed, including crystal structure refinement by the Rietveld method based on XRD data, along with investigations of its thermal expansion and ionic conductivity properties.

2. Experimental

The following reagents were used for the solid-state synthesis of $K_5Cu_{0.5}Hf_{1.5}(MoO_4)_6$: K_2CO_3 – analytical grade; CuO and HfO_2 – high purity; MoO_3 and K_2MoO_4 – chemically pure. $CuMoO_4$ was synthesized by annealing a stoichiometric mixture of CuO and MoO_3 at 350–500 °C for 50 hours. Hafnium molybdate was obtained via the reaction:

$$HfO_2 + 2\ MoO_3 = Hf(MoO_4)_2\ (500–750\ °C,\ 50\ hours)$$

The phase purity of the synthesized compounds was confirmed by XRD, and phase identification was performed by comparison with the ICDD PDF-2 [30].

XRD analysis was conducted using a D8 ADVANCE automated powder diffractometer (Bruker) equipped with a VANTEC detector, Cu$K\alpha$ radiation (λ = 1.5418 Å), reflection geometry, a secondary monochromator, and a scanning step size of 0.02076°. HT-XRD measurements were performed on the same instrument using an Anton Paar HTK16 high-temperature chamber over the 30–500 °C range, with 50 °C intervals. Structural refinement and unit cell parameter determination for $K_5Cu_{0.5}Hf_{1.5}(MoO_4)_6$ were carried out using the Topas 4.2 software package [31]. Thermal expansion tensor parameters were calculated and visualized using the TTT software suite [32]. The temperature dependence of the unit cell parameters was modeled using first and second degree polynomial approximations. Based on these data, the principal values of the thermal expansion tensor were determined, and cross-sectional plots of the thermal expansion coefficient surface were constructed.

ATR-FTIR spectra were recorded using a SIMEX FT-801 FT-IR spectrometer equipped with an attenuated total reflectance (ATR) accessory featuring a diamond crystal. Measurements were performed at room temperature over the 500–1100 cm^{-1} range with a resolution of 1 cm^{-1}.

Thermal analysis was carried out on an STA 449 F1 Jupiter thermoanalyzer (NETZSCH) using a platinum crucible, with a heating rate of 10 °C/min under an argon atmosphere over the temperature range of 30–800 °C.

EIS profiles of $K_5Cu_{0.5}Hf_{1.5}(MoO_4)_6$ were registered using a Z-1500J impedance analyzer (Elins, LLC) with an AC signal amplitude of 200 mV. Measurements were taken over a frequency range of 1 Hz to 1 MHz and a resistance range of 20 mΩ to 20 MΩ, within a temperature interval of 200–550 °C. For electrical characterization, the sample was fabricated as a pressed disk-shaped pellet (9 mm in diameter, 1.9 mm in height), sintered at 570 °C, and coated with platinum electrodes on the flat surfaces.

3. Results and discussion

3.1. Solid-state synthesis of $K_5Cu_{0.5}Hf_{1.5}(MoO_4)_6$

The single-phase polycrystalline form of the ternary molybdate $K_5Cu_{0.5}Hf_{1.5}(MoO_4)_6$ was synthesized by annealing stoichiometric mixtures of K_2MoO_4, $CuMoO_4$, and $Hf(MoO_4)_2$ at 350–550 °C for 150 hours.

According to XRD data, the formation of $K_5Cu_{0.5}Hf_{1.5}(MoO_4)_6$ from a stoichiometric mixture of simple molybdates proceeded through a sequential transformation pathway, with

the formation of potassium–hafnium binary molybdates as an intermediate stage:

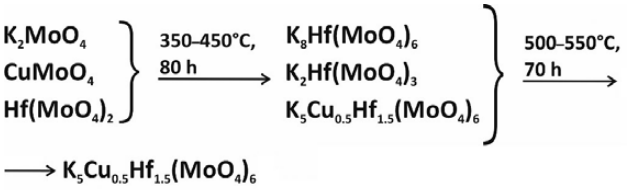

When simple oxides and potassium carbonate were used as starting materials, the reaction pathway become more complex. In this case, the intermediate phase $K_2Mo_3O_{10}$ persisted in the annealed products at temperatures up to 500 °C.

3.2. Rietveld refinement of $K_5Cu_{0.5}Hf_{1.5}(MoO_4)_6$

The crystal structure of $K_5Cu_{0.5}Hf_{1.5}(MoO_4)_6$ was refined using the Rietveld method, employing the atomic positional parameters of $Rb_5Co_{0.5}Hf_{1.5}(MoO_4)_6$ [27] as the initial structural model. Peak profiles were modeled using the Pearson VII function. The refinement was performed iteratively, with progressive addition of variables and simultaneous graphical background modeling. To reduce the number of refined parameters, the isotropic displacement factors (B_{iso}) for oxygen atoms were constrained to be equal.

The refinement process was stable and yielded low residual R-factors, which indicated good agreement between the experimental and calculated patterns. Final refinement results are presented in Table 1, selected interatomic distances in Table 2, and atomic coordinates along with isotropic displacement parameters in Table 3. The experimental, calculated, and

Table 1. Crystallographic parameters and structure refinement details for $K_5Cu_{0.5}Hf_{1.5}(MoO_4)_6$

Compound	$K_5Cu_{0.5}Hf_{1.5}(MoO_4)_6$
Space group	Trigonal, $R\bar{3}c$
a, Å	10.5617(2)
c, Å	37.5017(7)
V, Å^3	3622.9(1)
Z	6
2θ-interval, °	10–100
R_{wp}, %	3.78
R_p, %	3.01
R_{exp}, %	2.67
χ^2	1.42
R_B, %	1.35

Table 2. Selected interatomic distances (Å) in the crystal structure of $K_5Cu_{0.5}Hf_{1.5}(MoO_4)_6$

Tetrahedron MoO_4	
Mo–O1	1.854(16)
Mo–O2	1.852(11)
Mo–O3	1.727(17)
Mo–O4	1.670(12)
⟨Mo(1)–O⟩	1.776
Octahedron $(Cu1/Hf1)O_6$	
(Cu1/Hf1)–O1	2.017(16) ×6
Octahedron $(Cu2/Hf2)O_6$	
(Cu2/Hf2)–O2	2.087(13) ×6

Polyhedron $K1O_9$	
K1–O2	3.189(13) ×3
K1–O3	2.739(18) ×3
K1–O4	2.865(14) ×3
Polyhedron $K2O_{12}$	
K2—O1	3.368(12) ×2
K2—O1’	3.481(13) ×2
K2—O2	2.928(16) ×2
K2—O3	3.071(16) ×2
K2—O3’	3.328(12) ×2
K2—O4	2.866(12) ×2

Table 3. Atomic fractional coordinates and displacement parameters (Å^2) for $K_5Cu_{0.5}Hf_{1.5}(MoO_4)_6$

Atom	x	y	z	B_{iso}	Occ.
Cu1/Hf1	0	0	0	0.6(1)	$Cu_{0.15(1)}Hf_{0.85(1)}$
Cu2/Hf2	0	0	1/4	0.2(2)	$Cu_{0.35(1)}Hf_{0.65(1)}$
Mo	0.3504(3)	0.0565(2)	0.03253(5)	1.2(1)	
K1	0	0	0.3531(2)	4.5(3)	
K2	0.3801(7)	0	1/4	3.1(2)	
O1	0.163(1)	0.030(1)	0.0331(3)	1.3(2)	
O2	0.479(2)	0.238(1)	0.0518(3)	1.3(2)	
O3	0.353(2)	0.909(2)	0.0517(3)	1.3(2)	
O4	0.405(1)	0.058(1)	0.9907(3)	1.3(2)	

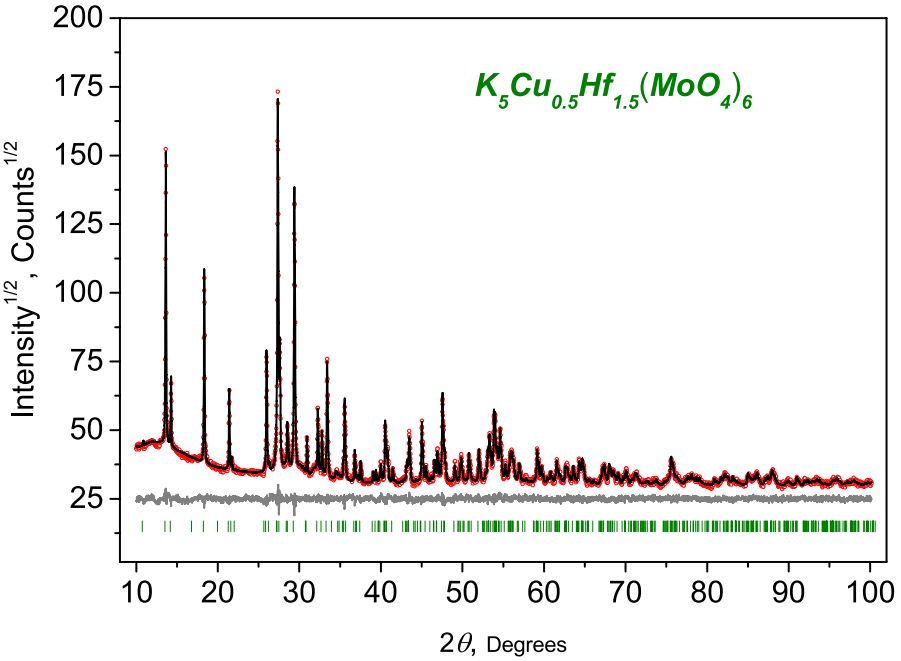

Fig. 1. Experimental (circles), calculated (solid line), difference, and dashed XRD patterns for $K_5Cu_{0.5}Hf_{1.5}(MoO_4)_6$

difference XRD patterns are shown in Figure 1.

Crystallographic data for $K_5Cu_{0.5}Hf_{1.5}(MoO_4)_6$ have been deposited with the Cambridge Crystallographic Data Centre under deposition number CSD 2386835 and are accessible at (www.ccdc.cam.ac.uk/data_request/cif).

The crystal structure of $K_5Cu_{0.5}Hf_{1.5}(MoO_4)_6$ consists of a three-dimensional framework formed by alternating, slightly distorted MoO_4 tetrahedra and two types of (Cu/Hf) octahedra, interconnected via shared oxygen vertices. Two distinct potassium cation sites are located within the spacious cavities of this framework (Figure 2).

Copper and hafnium atoms are statistically distributed over two special crystallographic sites: (Cu1/Hf1) and (Cu2/Hf2) with point symmetries 3 and 32, respectively. The (Cu1/Hf1) site is occupied by 0.85(1)Hf + 0.15(1)Cu, with an average (Cu1/Hf1)–O bond length of 2.017(16) Å. The (Cu2/Hf2) site contains 0.65(1)Hf + 0.35(1)Cu, with a corresponding (Cu2/Hf2)–O bond length of 2.087(16) Å. These Cu/Hf–O distances are comparable to the Hf–O bond lengths in the binary molybdate $K_8Hf(MoO_4)_6$, where Hf1–O1 = 2.0288 Å and Hf1–O12 = 2.0806 Å [33].

Molybdenum cations are coordinated by four oxygen atoms, forming MoO_4 tetrahedra with an average Mo–O bond length of 1.776 Å. The distortion of these tetrahedra is attributed to the differing local environments of the coordinating oxygen atoms. The longest Mo–O bonds are observed for O(2) and O(1), which also participate in the octahedral coordination of Cu and Hf cations. In contrast, the shortest Mo–O bonds

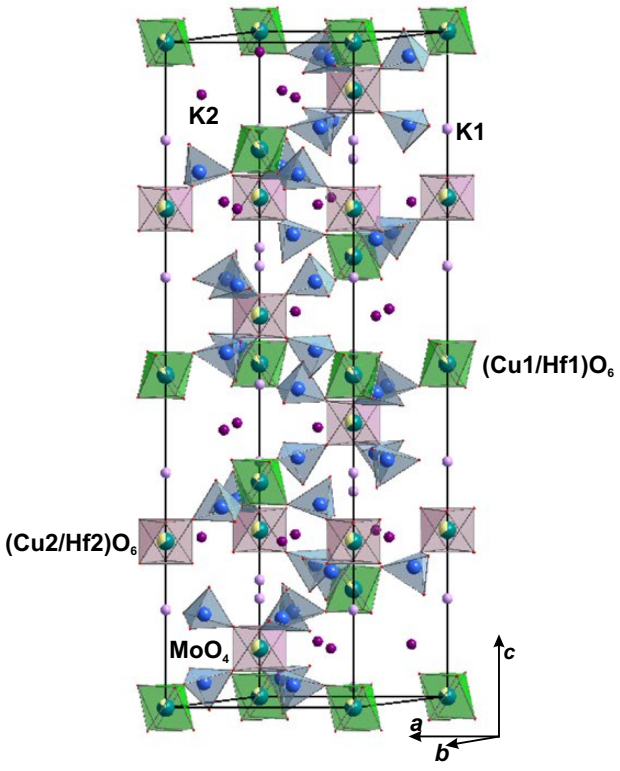

Fig. 2. Unit cell of $K_5Cu_{0.5}Hf_{1.5}(MoO_4)_6$

involve O(3) and O(4), which additionally bond to potassium cations located within the framework cavities. The potassium cations exhibit two distinct coordination environments: a $K1O_9$ nine-vertex polyhedron with <K1–O> bond lengths ranging from 2.739(18) to 3.189(13) Å, and a $K2O_{12}$ twelve-vertex polyhedron with bond lengths spanning 2.866(12) to 3.481(13) Å.

3.3. ATR-FTIR spectra

To elucidate the coordination environment of molybdenum atoms, ATR-FTIR absorption spectrum of $K_5Cu_{0.5}Hf_{1.5}(MoO_4)_6$ was recorded and is shown in Figure 3. In the vibrational spectra of molybdates, intense MoO_4 absorption bands typically appeared in the 700–980 cm^{-1} region, corresponding to symmetric and asymmetric stretching vibrations of Mo–O bonds within the MoO_4 tetrahedra. Additional bands in the 300–410 cm^{-1} range were attributed to O–Mo–O bending (deformation) modes [34].

Generally, the infrared spectra of molybdates are dominated by stretching vibrations of the MoO_4 tetrahedra. In the case of $K_5Cu_{0.5}Hf_{1.5}(MoO_4)_6$, ten distinct absorption bands were observed in the 500–1000 cm^{-1} range, all of which were assigned to internal vibrations of the MoO_4 tetrahedra (Table 4).

3.4. Thermal behavior

The thermal behavior of $K_5Cu_{0.5}Hf_{1.5}(MoO_4)_6$ was investigated using HT-XRD, DSC, and thermogravimetric analysis (TGA).

The DSC curve (Figure 4) displayed two endothermic events: a weak effect with a peak at 479 °C, and a more pronounced peak at 634 °C, corresponding to the melting of the compound. The TGA curve showed no mass loss over the studied temperature range. However, XRD analysis of the solidified melt revealed the presence of $CuMoO_4$, HfO_2, and $K_2Mo_4O_{13}$.

To clarify the origin of the endothermic effect at 479 °C, the sample was subjected to cyclic heating and cooling within the 200–600 °C range, remaining below the melting point. The endothermic peak was consistently reproduced on the heating curves in the range of 474–483 °C with high precision, while no thermal effects were observed on the corresponding cooling curves.

Table 4. Vibrational frequencies (cm^{-1}) observed in the ATR-FTIR spectrum of $K_5Cu_{0.5}Hf_{1.5}(MoO_4)_6$

Attribution	Vibration frequencies in the IR-spectr$K_5Cu_{0.5}Hf_{1.5}(MoO_4)_6$, cm^{-1}
$\nu_1(MoO_4)$	946, 926, 912
$\nu_2(MoO_4)$	898, 878, 848, 832, 806, 734, 714

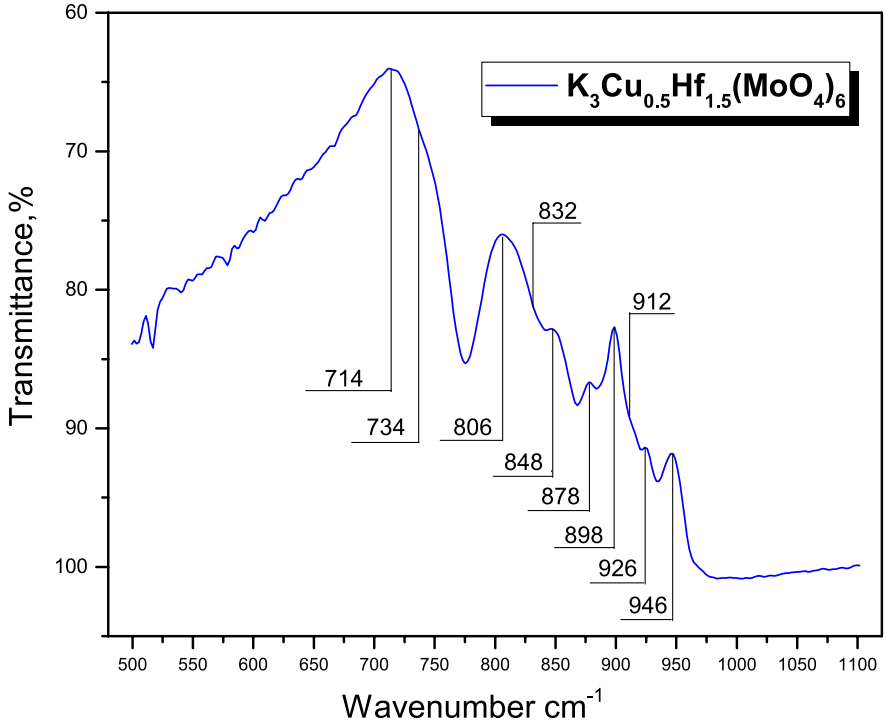

Fig. 3. ATR-FTIR absorption spectrum of $K_5Cu_{0.5}Hf_{1.5}(MoO_4)_6$

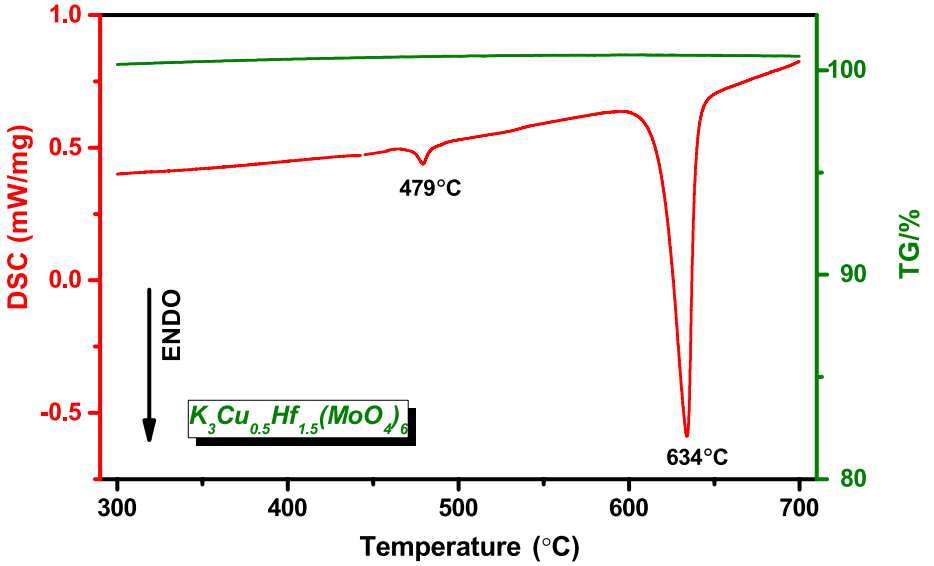

Fig. 4. TGA and DSC curves of $K_5Cu_{0.5}Hf_{1.5}(MoO_4)_6$

The temperature dependence of the unit cell parameters of $K_5Cu_{0.5}Hf_{1.5}(MoO_4)_6$, as determined by HT-XRD, is presented in Figure 7 and summarized in Table 5. Both lattice parameters, *a* and c, increased over the entire temperature range studied. The coefficients of thermal expansion (CTE), listed in Table 6, were calculated from polynomial approximations of the temperature-dependent trends in the lattice parameters and unit cell volume (Table 7). The *a* parameter and the unit cell volume were adequately described by linear fits. However, the *c* parameter displayed a distinct inflection between 400 and 500 °C, which coincided with the endothermic peak at 479 °C observed in the DSC curve, thereby requiring a second-degree polynomial approximation. A cross-sectional view of the thermal expansion tensor was compared with the *bc*-plane structural projection in Figure 8.

The coefficient α_a remained constant at $9.8 \cdot 10^{-6}$ °C^{-1} throughout the investigated

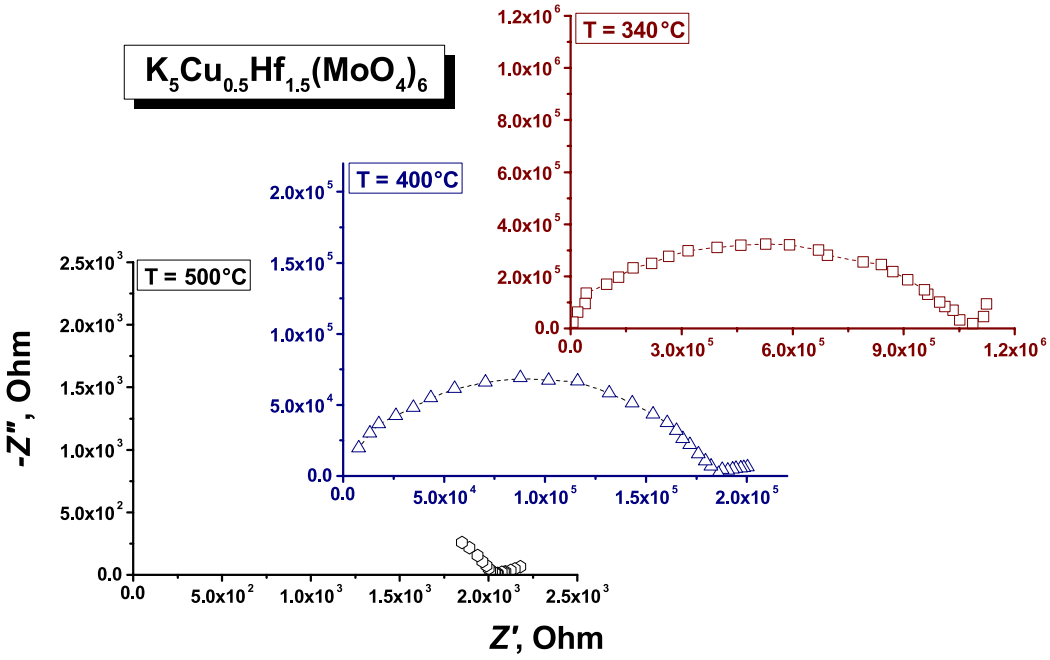

Fig. 5. EIS profiles of $K_5Cu_{0.5}Hf_{1.5}(MoO_4)_6$

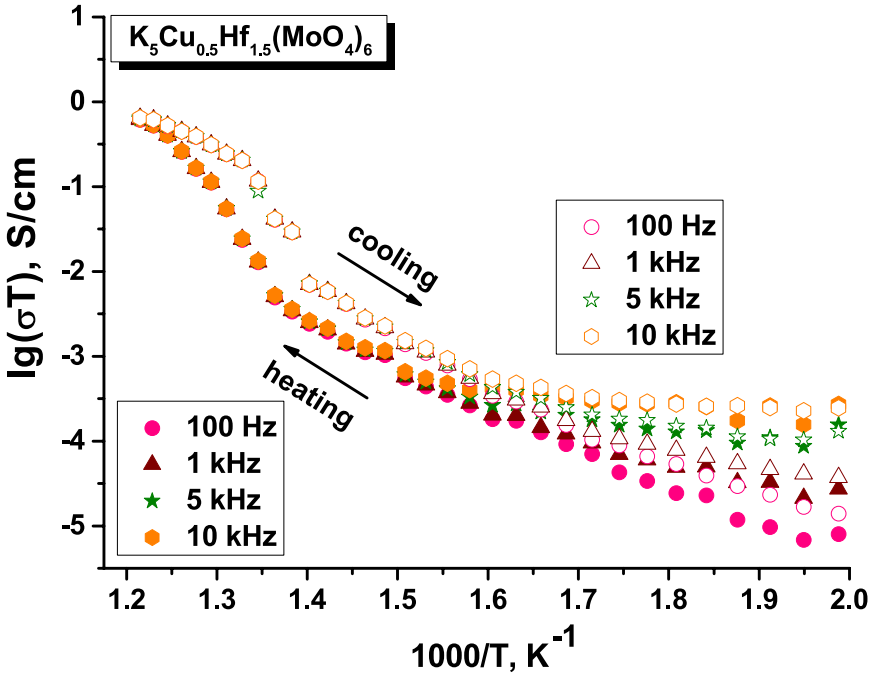

Fig. 6. Temperature dependence of the electrical conductivity of $K_5Cu_{0.5}Hf_{1.5}(MoO_4)_6$

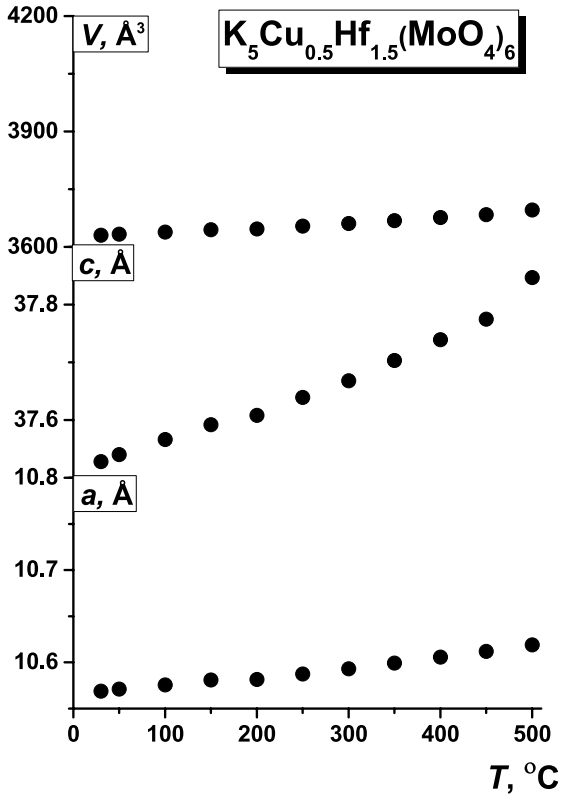

Fig. 7. Temperature dependence of lattice parameters for $K_5Cu_{0.5}Hf_{1.5}(MoO_4)_6$

Table 5. Unit cell parameters of $K_5Cu_{0.5}Hf_{1.5}(MoO_4)_6$ measured at various temperatures

T,°C	a, Å	c, Å	V, Å^3
30	10.5689(4)	37.528(2)	3630.3(4)
50	10.5710(3)	37.540(2)	3632.9(3)
100	10.5756(3)	37.566(1)	3638.6(2)
150	10.5810(4)	37.592(2)	3644.9(3)
200	10.5815(7)	37.608(3)	3646.8(5)
250	10.5874(4)	37.639(2)	3653.8(3)
300	10.5932(4)	37.668(2)	3660.6(3)
350	10.5994(5)	37.703(2)	3668.3(4)
400	10.6058(4)	37.739(2)	3676.3(3)
450	10.6119(4)	37.775(3)	3684.0(4)
500	10.6190(3)	37.847(2)	3696.0(3)

Table 6. Thermal expansion coefficients ($\times 10^{-6}$ °C^{-1}) for $K_5Cu_{0.5}Hf_{1.5}(MoO_4)_6$

T,°C	α_a	α_c	α_V
30	9.8(3)	8(2)	28(2)
50	9.8(3)	9(1)	28(2)
100	9.8(3)	11(1)	30(2)
150	9.8(3)	12.5(8)	32(2)
200	9.8(3)	14.4(5)	34(2)
250	9.8(3)	16.3(4)	36(2)
300	9.8(3)	18.2(5)	38(2)
350	9.8(3)	20.0(8)	40(2)
400	9.8(3)	22(1)	42(2)
450	9.8(3)	25(1)	43(2)
500	9.8(3)	26(2)	45(2)

Table 7. Temperature dependence of unit cell parameters approximated by linear and quadratic polynomial functions $a_0 + a_1 \times 10^{-3}t + a_2 \times 10^{-6}t^2$ in the range 30–500° C

Cell	a_0	a_1	a_2	R^2
a	10.565(1)	0.104(4)		1.00000
c	37.530(6)	0.26(7)	0.7(1)	0.99434
V	3625(2)	132(6)		1.00000

temperature range, indicating uniform expansion in the *ab*-plane. In contrast, α_c increased with temperature, ranging from $8 \cdot 10^{-6}$ °C^{-1} to $26 \cdot 10^{-6}$ °C^{-1}. The title compound exhibited relatively weak thermal expansion anisotropy, with the $\alpha_{max}/\alpha_{min}$ ratio varying from 1.2 to 2.7 depending on temperature (Table 8).

As with its isostructural analogs, $K_5Mn_{0.5}Zr_{1.5}(MoO_4)_6$ (space group *R*3c) [28] and $K_5Pb_{0.5}Zr_{1.5}(MoO_4)_6$ (space group $R\bar{3}c$) [29], the crystal structure of $K_5Cu_{0.5}Hf_{1.5}(MoO_4)_6$ can be described as a sequence of quasi-two-dimensional layers composed of $(Cu1/Hf1)O_6$ octahedra and MoO_4 tetrahedra. These layers are interconnected by $(Cu2/Hf2)O_6$ octahedra and twelve-vertex $K2O_{12}$ polyhedra (Figure 8). Thermal deformation in such framework materials is commonly interpreted using the concept of rigid unit modes (RUMs). These modes represent collective vibrational patterns responsible for the correlated rotation of rigid bodies within the framework, where the connectivity between "rigid" polyhedra is facilitated by relatively flexible bridging oxygen atoms [35]. Within this framework, thermal expansion in the *ab*-plane is primarily governed by interactions between rigid $Hf1O_6$ octahedra and MoO_4 tetrahedra and the more flexible $Cu1O_6$ octahedra. The expansion is driven by increasing deformation of Cu1–O bonds with temperature. The relatively weak anisotropy observed along the *c*-axis can be attributed to the presence of a greater number of deformable Cu2–O bonds in the interlayer space and the absence of rigid Mo–O linkages in this direction.

As shown in Table 8, the volumetric thermal expansion coefficient α_V of $K_5Cu_{0.5}Hf_{1.5}(MoO_4)_6$ reached 45×10^{-6} °C^{-1} at 500 °C, a value comparable to that of the isostructural zirconium analog $K_5Mn_{0.5}Zr_{1.5}(MoO_4)_6$ and approximately 30% lower than that of $K_5Pb_{0.5}Zr_{1.5}(MoO_4)_6$. This magnitude of α_V categorizes $K_5Cu_{0.5}Hf_{1.5}(MoO_4)_6$ as a material exhibiting high thermal expansion [36].

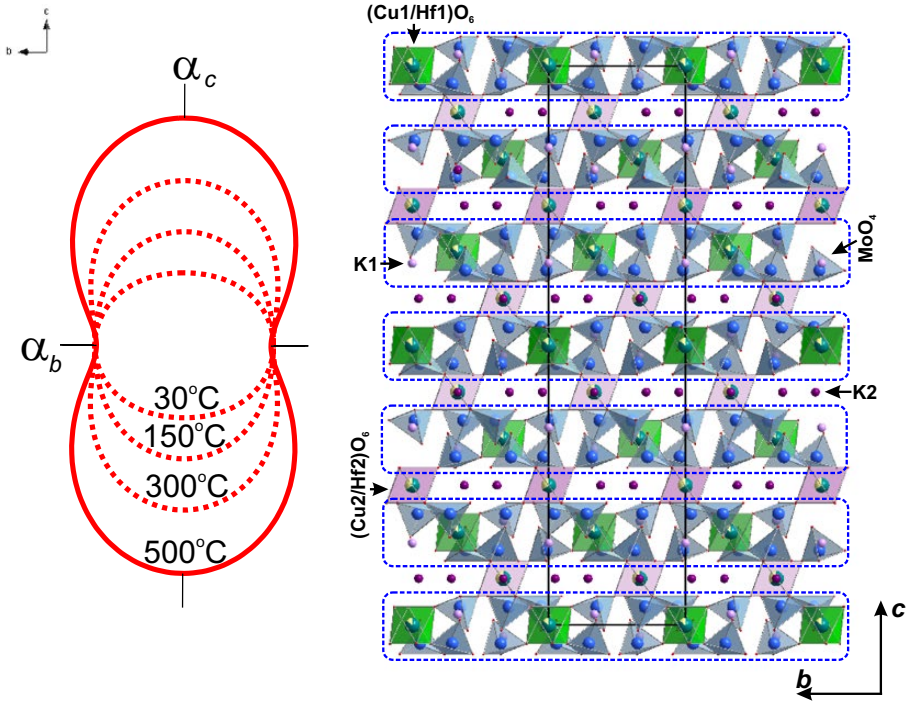

Fig. 8. Projection of the $K_5Cu_{0.5}Hf_{1.5}(MoO_4)_6$ crystal structure onto the *bc*-plane compared with cross sections of the thermal expansion tensor at 30, 150, 300, and 500 °C. Quasi-two-dimensional layers are highlighted by blue dashed lines

Table 8. Crystallographic parameters and thermal expansion coefficients of selected ternary molybdates with composition $K_5A_{0.5}E_{1.5}(MoO_4)_6$ (A = divalent, E = tetravalent element) [28, 29]

Compound	$K_5Cu_{0.5}Hf_{1.5}(MoO_4)_6$	$K_5Mn_{0.5}Zr_{1.5}(MoO_4)_6$	$K_5Pb_{0.5}Zr_{1.5}(MoO_4)_6$
Space group	$R\bar{3}c$	$R3c$	$R\bar{3}$
a, Å	10.5617(2)	10.6026(1)	10.6604 (2)
c, Å	37.5017(7)	37.6253(5)	37.9769 (9)
V, Å^3	3622.9(1)	3663.0(1)	3737.6 (2)
α_a, $\times10^{-6}$ °C^{-1} at 500°C	9.8(3)	10.9(2)	11.3(1)
α_c, $\times10^{-6}$ °C^{-1} at 500°C	26(2)	22(2)	37(2)
α_V, $\times10^{-6}$ °C^{-1} at 500°C	45(2)	43.7(1)	59.8(1)
$\alpha_{max}/\alpha_{min}$ at 500°C	2.7	2	3.3

Based on the results from HT-XRD and EIS (Section 3.5), the endothermic peak observed at 479 °C in the DSC curve is indicative of a first-order phase transition (Type I).

3.5. Electrical conductivity

The EIS profiles of $K_5Cu_{0.5}Hf_{1.5}(MoO_4)_6$, shown in Figure 5, displayed a single, high-frequency semicircle (or its segment at elevated temperatures, such as 500 °C, Figure 5). It represents the combined contribution of bulk and grain boundary conductivity. At lower frequencies, the plots exhibited a linear spike, indicative of ionic conduction and characteristic of the use of blocking electrodes.

The temperature dependence of the electrical conductivity of $K_5Cu_{0.5}Hf_{1.5}(MoO_4)_6$ is presented in Figure 6. A sharp increase in conductivity was observed at 473 °C, coinciding with the endothermic peak at 479 °C on the DSC curve (Figure 4), and corresponding to a polymorphic phase transition. The cooling curve revealed a pronounced thermal hysteresis, consistent with a first-order phase transition.

Below the transition temperature, the activation energy E_a = 0.8 eV, and the conductivity reaches $2.4\cdot10^{-7}$ S/cm at 300 °C. Above the transition, the activation energy increased slightly to 0.9 eV, with the conductivity reaching $7.5\cdot10^{-4}$ S/cm at 550°C.

4. Conclusion

A novel ternary molybdate $K_5Cu_{0.5}Hf_{1.5}(MoO_4)_6$ was successfully synthesized via solid-state reaction, expanding the family of isostructural compounds with the general formula $M^{I}_5M^{II}_{0.5}M^{IV}_{1.5}(MoO_4)_6$. The sequence of chemical transformations leading to the formation of the potassium–copper–hafnium molybdate from a stoichiometric mixture of simple molybdates was elucidated. The compound's thermal stability was evaluated, and its crystal structure was refined using the Rietveld method within the trigonal space group $R\bar{3}c$. The coordination environment of molybdenum atoms was confirmed by ATR-FTIR spectroscopy, which revealed characteristic vibrational bands of MoO_4 tetrahedra. HT-XRD analysis demonstrated that $K_5Cu_{0.5}Hf_{1.5}(MoO_4)_6$ exhibited pronounced thermal expansion, categorizing it as a high thermal expansion material. The compound's ion-conducting properties were also investigated, with conductivity reaching $7.5\cdot10^{-4}$ S/cm at 550 °C with an activation energy of E_a = 0.9 eV. Combined evidence from HTXRD and EIS indicated that the endothermic effect observed at 479 °C in the DSC curve corresponded to a first-order phase transition.

Contribution of the authors

The authors contributed equally to this article.

Conflict of interests

The authors declare that they have no known competing financial interests or personal relationships that could have influenced the work reported in this paper.

References

1. Ben N. W., Ben R. A. Ferroelectric properties and alternative current conduction mechanisms of lithium rubidium molybdate. *Ionics*. 2019;25: 4003–4012. https://doi.org/10.1007/s11581-019-02921-w

2. Tsyrenova G. D., Pavlova E. T., Solodovnikov S. F., … Lazoryak B. I. New ferroelastic $K_2Sr(MoO_4)_2$: synthesis, phase transitions, crystal and domain structures, ionic conductiv-

ity. *Journal of Solid State Chemistry*. 2016;237: 64–71. https://doi.org/10.1016/j.jssc.2016.01.011

3. Spassky D., Vasil'ev A., Jamal M. U., … Nagirnyi V. Temperature dependent energy transfer to Eu^{3+} emission centres in $K_5Eu(MoO_4)_4$ crystals. *CrystEngComm*. 2024;26(8): 1106–1116. https://doi.org/10.1039/d3ce01201h

4. Wang J., Luo L., Huang B., … Wang J. The preparation and optical properties of novel $LiLa(MoO_4)_2$:Sm^{3+},Eu^{3+} red phosphor. *Materials*. 2018;11(2): 297. https://doi.org/10.3390/ma11020297

5. Loiko P., Pavlyuk A., Slimi S., … Mateos X. Growth, spectroscopy and laser operation of monoclinic Nd:$CsGd(MoO_4)_2$ crystal with a layered structure. *Journal of Luminescence*. 2021;231: 117793. https://doi.org/10.1016/j.jlumin.2020.117793

6. Binish B., Durairaj M., Girisun Sabari T. C., Mani Rahulan K. Engineering the nonlinear optical properties of barium molybdate by doping Sn^{4+} ions for optical limiting device applications, *Ceramics International*. 2023;49(11): 17629–17638. https://doi.org/10.1016/j.ceramint.2023.02.129

7. Nasri R., Larbi T., Amlouk M., Zid M. F. Investigation of the physical properties of $K_2Co_2(MoO_4)_3$ for photocatalytic application. *Journal of Materials Science: Materials in Electronics*. 2018;29: 18372–18379. https://doi.org/10.1007/s10854-018-9951-x

8. Chimitova O. D., Bazarov B. G., Bazarova J. G., … Ehrenberg H. The crystal growth and properties of novel magnetic double molybdate $RbFe_5(MoO_4)_7$ with mixed Fe^{3+}/Fe^{2+} states and 1D negative thermal expansion. *CrystEngComm*. 2021;23: 3297–3307. https://doi.org/10.1039/D1CE00118C

9. Liu M., Zhang Y., Zou T., Garlea V. O., … Liu J.-M. Antiferromagnetism of double molybdate $LiFe(MoO_4)_2$. *Inorganic Chemistry*. 2020;59: 8127–8133. https://doi.org/10.1021/acs.inorgchem.0c00432

10. Grossman V. G., Molokeev M. S., Bazarov B. G., Bazarova J. G. Potassium and thallium conductors with a trigonal structure in the M_2MoO_4–$Cr_2(MoO_4)_3$–$Hf(MoO_4)_2$ (M = K, Tl) systems: synthesis, structure, and ionic conductivity. *Journal of Alloys and Compounds*. 2021;873: 159828. https://doi.org/10.1016/j.jallcom.2021.159828

11. Savina A. A., Morozov V. A., Buzlukov A. L., … Khaikina E. G. New solid electrolyte $Na_9Al(MoO_4)_6$: structure and Na^+ ion conductivity. *Chemistry of Materials*. 2017;29: 8901–8913. https://doi.org/10.1021/acs.chemmater.7b03989

12. Spiridonova T. S., Solodovnikov S. F., Molokeev M. S., … Khaikina E..G. Synthesis, crystal structures, and properties of new acentric glaserite-related compounds $Rb_7Ag_{5-3x}Sc_{2+x}(XO_4)_9$ (X = Mo, W). *Journal of Solid State Chemistry*. 2022;305: 122638. https://doi.org/10.1016/j.jssc.2021.122638

13. Solodovnikov S. F., Solodovnikova Z. A., Zolotova E. S., … Kuchumov B. M. Nonstoichiometry in the systems Na_2MoO_4–$MMoO_4$ (M = Co, Cd), crystal structures of $Na_{3.36}Co_{1.32}(MoO_4)_3$, $Na_{3.13}Mn_{1.43}(MoO_4)_3$ and $Na_{3.72}Cd_{1.14}(MoO_4)_3$, crystal chemistry, compositions and ionic conductivity of alluaudite-type double molybdates and tungstates. *ournal of Solid State Chemistry*. 2017;253: 121–128. https://doi.org/10.1016/j.jssc.2017.05.031

14. Kotova I. Y., Belov D. A., Stefanovich S. Y. $Ag_{1-x}Mg_{1-x}R_{1+x}(MoO_4)_3$ Ag+-conducting nasicon-like phases, where R = Al or Sc and $0 \leqslant x \leqslant 0.5$. *Russian Journal of Inorganic Chemistry*. 2011;56: 1189–1193. https://doi.org/10.1134/S0036023611080122

15. Buzlukov A. L., Fedorov D. S., Serdtsev A. V., … Medvedeva N..I. Ion mobility in triple sodium molybdates and tungstates with a NASICON structure. *Journal of Experimental and Theoretical Physics*. 2022;134: 42–50. https://doi.org/10.1134/S1063776122010071

16. Xu D., Zhang H., Pang L., … Zhou D. Novel B-site scheelite structure ceramic $Bi(Ge_{0.5}Mo_{0.5})O_4$ and its dielectric properties. *Journal of the American Ceramic Society*. 2023;106 (11): 6675–6683. https://doi.org/10.1111/jace.19282

17. Solodovnikov S. F., Gulyaeva O. A., Savina A. A., … Denisova T. A. Molybdates and tungstates of the alluaudite family: crystal chemistry, composition, and ionic mobility. *Journal of Structural Chemistry*. 2022;63: 1101–1133. https://doi.org/10.1134/S0022476622070071

18. Spiridonova T. S., Solodovnikov S. F., Molokeev M. S., … Khaikina E. G. Synthesis, crystal structures, and properties of new acentric glaserite-related compounds $Rb_7Ag_{(5-3x)}Sc_{(2+x)}(XO_4)_9$ (X = Mo, W). *Journal of Solid State Chemistry*. 2022;305: 122638. https://doi.org/10.1016/j.jssc.2021.122638

19. Bugaris D. E., Loye H.-C. $Li_3Al(MoO_4)_3$, a lyonsite molybdate. *Acta Crystallographica Section C Crystal Structure Communications*. 2012;C68: i34–i36. https://doi.org/10.1107/S0108270112020513

20. Grossman V. G., Molokeev M. S., Bazarov B. G., Bazarova J. G. Synthesis and characterization of a new magnesium molybdates $Tl_{1.85}M_{0.15}Mg_2(MoO_4)_3$ (M = K, Rb) with a langbeinite type structure. *Solid State Sciences*. 2023;142: 107249. https://doi.org/10.1016/j.solidstatesciences.2023.107249

21. Klevtsova R. F., Bazarova Zh. G., Glinskaya L. A., … Fedorov K. N. Synthesis of ternary potassium, magnesium, and zirconium molybdates. The crystal structure of $K_5(Mg_{0.5}Zr_{1.5})\cdot(MoO_4)_6$. *Journal of Structural Chemistry*. 1994;35: 286–290. https://doi.org/10.1007/BF02578278

22. Klevtsova R. F., Bazarova Zh. G., Glinskaya L. A., Bazarov B. G., Fedorov K. N., Klevtsov P. V. Crystal structure investigation of ternary molybdate $K_5(Mn_{0.5}Zr_{1.5})\cdot(MoO_4)_6$. *J Struct Chem*. 1995;36: 813–817. https://doi.org/10.1007/BF02579674

23. Klevtsova R. F., Bazarov B. G., Glinskaya L. A., … Bazarova Zh. G. Synthesis and X-ray study of single crystals of $K_5(Cd_{0.5}Zr_{1.5})(MoO_4)_6$ triple molybdate. *J Struct Chem*. 2002;43: 939–943. https://doi.org/10.1023/A:1023686325616

24. Grossman V. G., Molokeev M. S., Bazarova J. G., Bazarov B. G. High ionic conductivity of $K_{5-x}Tl_x(Mg_{0.5}Hf_{1.5})(MoO_4)_6$ ($0 \leqslant x \leqslant 5$) solid solutions. *Solid State Sciences*. 2022;134: 107027. https://doi.org/10.1016/j.solidstatesciences.2022.107027

25. Bazarov B. G., Klevtsova R. F., Sarapulova A. E., Fedorov K. N., Glinskaya L. A., Bazarova Zh. G. Synthesis and crystal structure of ternary molybdate compound $K_5Pb_{0.5}Hf_{1.5}(MoO_4)_6$. *Journal of Structural Chemistry*. 2005;46: 756–760. https://doi.org/10.1007/s10947-006-0197-8

26. Bazarov B. G., Sarapulova A. E., Klevtsova R. F., Glinskaya L. A., Fedorov K. N., Bazarova Zh. G. Synthesis, structure and vibration spectra of the triple molybdates $Tl_5A_{0.5}Hf_{1.5}(MoO_4)_6$, A = Ca, Sr, Ba, Pb. *Journal of Alloys and Compounds*. 2008;448 (1–2): 325–330. https://doi.org/10.1016/j.jallcom.2006.11.086

27. Aksenov S. M., Pavlova Er. T., Popova N. N., Tsyrenova G. D., Lazoryak B. I. Stoichiometry and topological features of triple molybdates $A_xB_yC_z(MoO_4)_n$ with the heteropolyhedral open MT-frameworks: synthesis, crystal structure of $Rb_5\{Hf_{1.5}Co_{0.5}(MoO_4)_6\}$, and comparative crystal chemistry. *Solid State Sciences*. 2024;151: 107525. https://doi.org/10.1016/j.solidstatesciences.2024.107525

28. Kovtunets E. V., Tushinova Yu. L., Logvinova A. V., Bazarova Ts. T., Bazarov B. G. Thermal expansion of ternary molybdate $K_5[Mn_{0.5}Zr_{1.5}](MoO_4)_6$. *ESSUTM Bulletin*. 2024;3(94): 90–97. https://doi.org/10.53980/24131997_2024_3_90

29. Kovtunets E. V., Spiridonova T. S., Tushinova Yu. L., Logvinova A. V., Bazarova Ts. T., Bazarov B. G. Thermal expansion and ionic conductivity of $K_5Pb_{0.5}Zr_{1.5}(MoO_4)_6$. *Proceedings of Universities. Applied Chemistry and Biotechnology*. 2024;14(4): 444–452. https://doi.org/10.21285/achb.939 (In Russ.)

30. ICDD PDF-2 Database, Cards № 01-072-0735, 01-073-0488, 01-077-0699, 01-083-2240.

31. Coelho A. A. TOPAS and TOPAS-Academic: an optimization program integrating computer algebra and crystallographic objects written in C++. *Journal of Applied Crystallography*. 2018;51: 210–218. https://doi.org/10.1107/S1600576718000183

32. Bubnova R. S., Firsova V. A., Filatov S. K. Software for determining the thermal expansion tensor and the graphic representation of its characteristic surface (theta to tensor-TTT). *Glass Physics and Chemistry*. 2013;39: 347–350. https://doi.org/10.1134/S108765961303005X

33. Klevtsova R. F., Glinskaya L. A., Pasechnyuk N. P. Crystal structure of the binary molybdates $K_8Zr(MoO_4)_6$ and $K_8Hf(MoO_4)_6$. *Kristallografiya*. 1977;22: 1191–1195. (In Russ.)

34. Fomichev V. V., Poloznikova M. E., Kondratov O. I. Structural features and spectroscopic and energy characteristics of alkali metal molybdates and tungstates. *Russian Chemical Reviews* 1992;61(9): 877–888. https://doi.org/10.1070/RC1992v061n09ABEH001004

35. Petrushina M. Y., Korenev S. V., Dedova E. S., Gubanov A. I. Materials AM_2O_8 (A = Zr, Hf; M = W, Mo) with negative thermal expansion. *J. Struct. Chem*. 2020;61: 1655–1680. https://doi.org/10.1134/S0022476620110013

36. Pet'kov V. I., Shipilov A. S., Sukhanov M. V. Thermal expansion of $MZr_2(AsO_4)_3$ and $MZr_2(TO_4)_x(PO_4)_{3-x}$ (M = Li, Na, K, Rb, Cs; T = As, V). *Inorganic Materials*. 2015;51(11): 1079–1085. https://doi.org/10.1134/S002016851510012X

Information about the authors

Evgeniy V. Kovtunets, Cand. Sci. (Phys.–Math.), Researcher, Laboratory of Oxide Systems, Baikal Institute of Nature Management, Siberian Branch of the Russian Academy of Sciences (Ulan-Ude, Russian Federation).
https://orcid.org/0000-0003-1301-1983
kovtunets@binm.ru

Tatiyana S. Spiridonova, Cand. Sci. (Chem.), Senior Researcher, Laboratory of Oxide Systems, Baikal Institute of Nature Management, Siberian Branch of the Russian Academy of Sciences (Ulan-Ude, Russian Federation).
https://orcid.org/0000-0001-7498-5103
spiridonova@binm.ru

Yunna L. Tushinova, Cand. Sci. (Chem.), Researcher, Laboratory of Oxide Systems, Baikal Institute of Nature Management, Siberian Branch of the Russian Academy of Sciences (Ulan-Ude, Russian Federation).
https://orcid.org/0000-0003-1032-8854
tushinova@binm.ru

Tsyrendyzhit T. Bazarova, Cand. Sci. (Chem.), Lead Engineer, Laboratory of Oxide Systems, Baikal Institute of Nature Management, Siberian Branch of the Russian Academy of Sciences (Ulan-Ude, Russian Federation).
https://orcid.org/0000-0001-9697-6320
basst@list.ru

Alexandra V. Logvinova, Engineer, Laboratory of Oxide Systems, Baikal Institute of Nature Management, Siberian Branch of the Russian Academy of Sciences (Ulan-Ude, Russian Federation).
https://orcid.org/0000-0001-9850-2719
logvinova_alexsandra@bk.ru

Bair G. Bazarov, Dr. Sci. (Phys.–Math.), Leading Researcher, Laboratory of Oxide Systems, Baikal Institute of Nature Management, Siberian Branch of the Russian Academy of Sciences (Ulan-Ude, Russian Federation).
https://orcid.org/0000-0003-1712-6964
bazbg@rambler.ru

Received October 23, 2024; approved after reviewing November 11, 2024; accepted for publication November 15, 2024; published online September 25, 2025.